Mechanical Properties of Vacancy-containing Graphene and Graphite using Molecular Dynamics Simulations

Akihiko Ito and Shingo Okamoto

Abstract—**We investigated the mechanical properties of graphene and graphite containing vacancies under tensile loading using molecular dynamics (MD) simulations. In the MD simulations, we used two types of potential functions: the second-generation reactive empirical bond-order (REBO) potential for covalent C–C bond, and the Lennard-Jones potential for the interlayer interaction of graphite. The influence of the size and the distributional form of vacancies on the mechanical properties of graphene and graphite were studied. It was found that the tensile strength of graphene having randomly distributed vacancies with a vacancy density of 4%, decreased by 59%.**

Index Terms—**Graphene, graphite, molecular dynamics, vacancy**

I. Introduction

CARBON-based materials can have excellent mechanical and electrical properties. Therefore, there is much interest around their use in applications in structural sub-assemblies and nano-electro mechanical systems such as electrochemical electrodes and field emission. Carbon materials such as diamond, graphene, carbon nanotubes (CNT), and fullerenes, have a wide range of excellent properties thanks to their different types of bonds and atomistic structures. In particular, graphene has rigidity and strength that are nearly equal to those of diamond, as well as novel electronic properties including high electron mobility. Thus, studies on graphene and graphite made of graphene layers have recently intensified [1]–[3].

Defects often affect the mechanical and electronic properties of materials. There have been reports of experimental studies on defects (i.e., vacancies [4], dislocations [5], and grain boundaries [6]) in graphene layers. It is important to clarify the influence of defects on the mechanical and electrical properties of graphene and graphite in order to produce high-performance carbon materials.

Recently, studies aiming to clarify the relationship between atomic-scale defects and mechanical properties have increased in number. The tensile properties of graphene and carbon nanotubes containing multiple Stone-Wales (SW) defects have been investigated using molecular dynamics (MD) simulations by Xiao *et al.* [7]. These studies have clarified the relationship between the number of defects and the mechanical properties. The influence of grain boundaries on the tensile strength of graphene has been investigated by Grantab *et al.* [8]. The MD simulations of tensile loadings of single-walled carbon nanotubes with vacancies have been performed by Wong *et al.* [9]. The influence of the single and double vacancies on the tensile strength has been investigated through molecular mechanics (MM) calculations by Zhang *et al.* [10]. Zhang *et al.* compared their results obtained using MM calculations with Mielke's results obtained using quantum mechanics (QM) calculations [11]. However, the influence of vacancies on the mechanical properties of graphene and graphite were neglected. In this study, we investigated the influence of vacancy size on the mechanical properties of graphene and graphite through MD simulations. In addition, we clarified the relationship between the distributional form of vacancies and the mechanical properties.

Manuscript received December 14, 2011. This work was supported in part by the Ring-Ring project of JKA.

Akihiko Ito is with the Mechanical Engineering Course, Graduate School of Science and Engineering, Ehime University, 3 Bunkyo-cho, Matsuyama 790-8577, Japan. He is also with the Composite Materials Research Laboratories, Toray Industries, Inc., Masaki-cho 791-3193, Japan (e-mail: Akihiko_Ito@nts.toray.co.jp).

Shingo Okamoto is with the Mechanical Engineering Course, Graduate School of Science and Engineering, Ehime University, 3 Bunkyo-cho, Matsuyama 790-8577, Japan (e-mail: okamoto.shingo.mh@ehime-u.ac.jp).

II. Method

A. Potential Function

In the present study, we used two types of interatomic potentials: the second-generation reactive empirical bond order (2nd REBO) [12], and Lennard-Jones potentials. The 2nd REBO potential for covalent C-C bonds is expressed as

$$E_{REBO} = \sum_i \sum_{j>i} \left[V_R(r_{ij}) - B_{ij}^* V_A(r_{ij}) \right], \tag{1}$$

where r_{ij} represents the distance between atoms i and j. The B_{ij}^* represents the bond-order term. The terms $V_R(r_{ij})$ and $V_A(r_{ij})$ represent the pair-additive interactions that reflect interatomic repulsions and attractions, respectively as in

$$\begin{aligned} V_R(r) &= f_c(r)\left(1+\frac{Q}{r}\right) A \exp(-\alpha r) \\ V_A(r) &= f_c(r) \sum_{n=1}^{3} B_n \exp(-\beta_n r) \end{aligned}, \tag{2}$$

ISBN: 978-988-19251-1-4
ISSN: 2078-0958 (Print); ISSN: 2078-0966 (Online)

where Q, A, α, B_n, and β_n represent constant parameters. The function $f_c(r)$ represents the cutoff function that decreases monotonously from 1 to 0 as in

$$f_c(r)=\begin{cases}1, & r<R_{\min}\\ \left\{1+\cos\left[\dfrac{\pi(r-R_{\min})}{R_{\max}-R_{\min}}\right]\right\}/2, & R_{\min}<r<R_{\max}\\ 0, & r>R_{\max}\end{cases}, \quad (3)$$

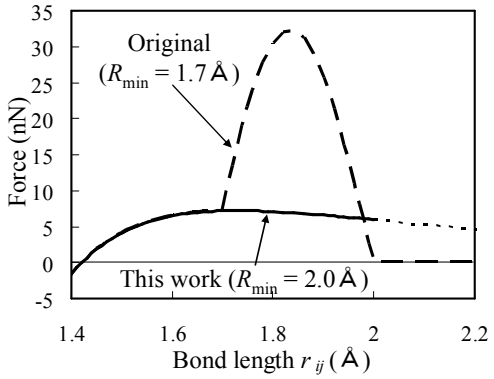

Fig. 1 Interatomic forces for 2nd REBO potential with original $R_{\min}$ and $R_{\min}$ used in this work.

where $R_{\min}$ = 1.7 Å and $R_{\max}$ = 2.0 Å in original 2nd REBO potential.

It is known that for the original 2nd REBO potential, the interatomic force increases dramatically at $r = R_{\min}$ and reaches zero at $r = R_{\max}$ owing to the discontinuity in the second derivative of the cutoff function, as shown in Fig. 1. This dramatic increase in the interatomic force with the original 2nd REBO potential may greatly affect tensile strength. Therefore, in this work, the cutoff parameter is set to 2.0 Å in order to avoid the dramatic increase in the interatomic force [13]. The other parameters, except for $R_{\min}$, are set to the values proposed by Brenner [12]. The Lennard-Jones potential for the interlayer interaction in the graphite model is expressed as

$$V^{LJ}=4\varepsilon\left[\left(\frac{r_0}{r_{ij}}\right)^{12}-\left(\frac{r_0}{r_{ij}}\right)^{6}\right]. \quad (4)$$

The 2nd REBO potential and the Lennard-Jones potential are switched according to the interatomic distance and bond order [14]. The value of ε is set to 0.00284 eV and r_0 is set to 3.2786 Å so that the interplanar spacing of graphite at 300 K is 3.35 Å, which is a known experimental value.

B. Analysis model

Firstly, the analysis models of graphene used under zigzag tensions consist of 588 carbon atoms with dimensions equal to those of the real crystallite in a typical carbon material, as shown in Fig. 2.

No periodic boundary conditions are imposed in our case. The analysis models consist of two parts. One is referred to as the active zone in which the atoms move according to the interactions with their neighboring atoms. The other—enclosed within the boxes (as shown in Fig. 2)—is referred to as the boundary zone in which the atoms are restrained. The thickness l of the boundary zone is 3.0a for the armchair tension model and $1.5\times\sqrt{3}a$ for the zigzag tension model, where a is the length of the C=C bond in graphene.

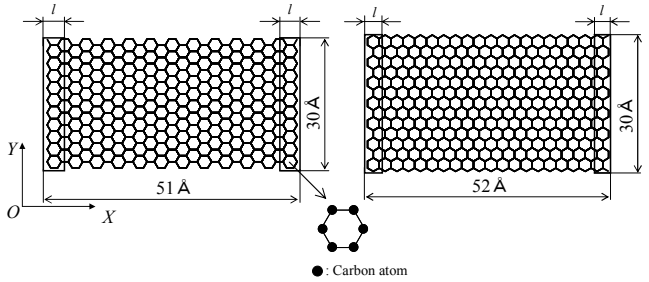

(a) Armchair tension model (b) Zigzag tension model

Fig. 2 Configurations of graphene used under zigzag tension.

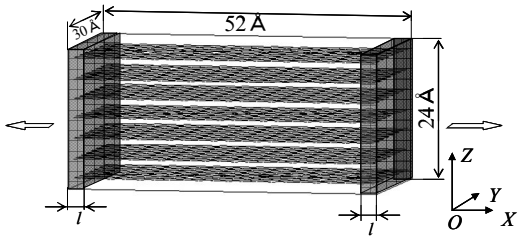

Fig. 3 Configuration of graphite used under zigzag tension.

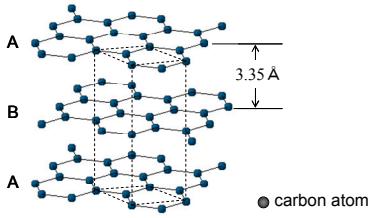

Fig. 4 Schematic of graphite structure.

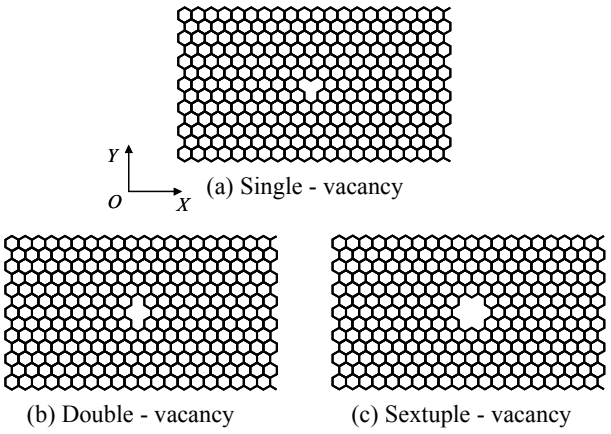

(a) Single - vacancy

(b) Double - vacancy (c) Sextuple - vacancy

Fig. 5 Analysis model for the graphene containing a cluster-type vacancy.

The analysis model of graphite used under zigzag tension consists of 4,116 carbon atoms with dimensions equal to those of the real crystallite in typical carbon material, as shown in Fig. 3. The graphite model is made of seven layers of graphene sheets, which are stacked in an AB-type sequence with an interlayer spacing of 3.35 Å, as shown in Fig. 4.

The analysis models of graphene with cluster-type vacancies are shown in Fig. 5. These models of graphite

ISBN: 978-988-19251-1-4
ISSN: 2078-0958 (Print); ISSN: 2078-0966 (Online)

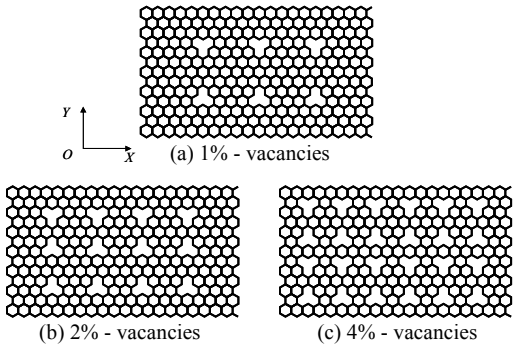

Fig. 6 Analysis model for the graphene containing uniformly distributed vacancies.

reveal that the graphene sheet with a cluster-type vacancy is always the center layer.

The analysis models of graphene containing uniformly distributed vacancies are shown in Fig. 6. Each vacancy is a single vacancy and set so that the distance between neighboring vacancies is identical. Calculations for three values of vacancy density, namely 1, 2, and 4%, are performed.

The analysis models of graphene containing randomly distributed vacancies are set by removing carbon atoms in the active zone using a pseudorandom number generator.

C. Molecular dynamics simulations

We investigated the mechanical properties of vacancy-containing graphene and graphite using the MD simulations under constant volume and temperature, that is, a canonical (NVT) ensemble. The Verlet method is used for the time integral of the equations of motion of atoms. The velocities of all atoms are adjusted simultaneously using the velocity scaling method [15] so that the temperature of the object can be maintained at the preset temperature T_{SET}. The mass of a single carbon atom, m, is 1.9927×10^{-26} kg. The time step is 1.0 fs.

The atomic stress acting on each atom is calculated to obtain the stress-strain curves and to visualize the stress distribution during tensile loadings. The atomic stress $\sigma^i{}_J$ for each of the X, Y, and Z directions of J is given by calculating the kinetic energies of, the interatomic force acting on, and the volume occupied by atom i as in

$$\sigma^i{}_J = \frac{1}{\Omega^i}\left(m\overline{V^i{}_J V^i{}_J} + \overline{J^i F^i{}_J}\right), \quad (5)$$

where Ω^i represents the volume occupied by atom i, which is referred to as the atomic volume. The atomic volume is calculated by averaging the volume over all atoms in the initial structure of each system. The interatomic force acting on atom i due to its neighboring atoms is represented by F^i. The global stress of an analysis model is calculated by averaging over all carbon atoms in each system.

Method of tension loading

The initial positions of the atoms are given so that the analysis model represents the crystal structure of graphene or graphite at a preset temperature. First, the atoms in the active zone of the analysis model are relaxed in unloaded states for 7,000 MD steps. The atoms in the boundary zone are fixed. After constant displacements are applied to the atoms in both of the boundary zones to simulate uniaxial tensile loading in the X direction, the atoms in the active zone are relaxed for 7,000 MD steps. The strain increment, $\Delta\varepsilon$, is 0.004. The output stresses are sampled for the last 2,000 MD steps for each strain and are averaged. Young's moduli are obtained from the slopes of the straight lines in the range where the relationship between the stress and strain is linear, and tensile strengths are given by the last peak of the nominal stress-nominal strain curves.

III. Results and Discussion

A. Validation of calculation method

We performed the MD simulations on tensile loadings of pristine graphene at 300 K to verify the propriety of our calculation method. The results are presented in Table I and Fig. 7. The average tensile strength is 83 GPa, which is in agreement with the 121 GPa calculated by Pei *et al.* through MD simulations [16] and the experimentally obtained value of 123.5 GPa [1]. The average Young's modulus is 836 GPa, which is within the range of results obtained by the DFT method [17] (1,050 GPa) and by experiment [18] (500 GPa and 1 TPa). It is estimated that the lower value obtained in this work is due to the effect of size on the elastic properties of graphene [18].

TABLE I
Mechanical Properties of Pristine Graphene

Direction	Tensile strength (GPa)	Young's modulus (GPa)
Armchair	76	879
Zigzag	91	794
Average	83	836

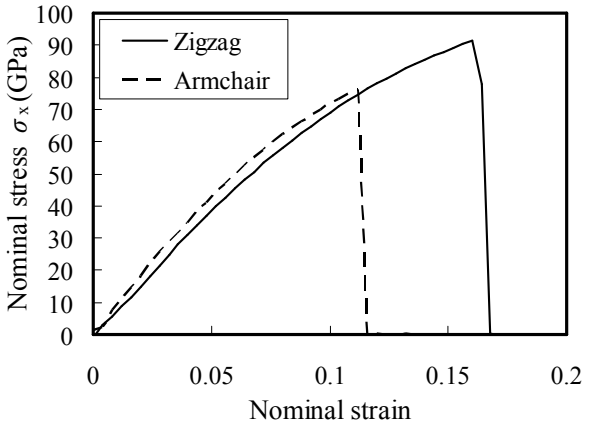

Fig. 7 Stress-strain curves of pristine graphene under Armchair or Zigzag tension.

B. Mechanical properties of vacancy-containing graphene

The mechanical properties of vacancy-containing graphene obtained at 300 K are listed in tables II and III, together with the results from previous studies on carbon nanotubes

ISBN: 978-988-19251-1-4
ISSN: 2078-0958 (Print); ISSN: 2078-0966 (Online)

[9]–[11]. The nominal stress-nominal strain curves of the graphene are given in Fig. 8. The results for pristine graphene are also given for reference. The decrease in the tensile strength is larger for graphene with double vacancy, followed by that of the sextuple and then single vacancy. In addition, the fracture strain for graphene with double vacancy is the least. The decrease in tensile strength relative to that of pristine graphene is 29, 28, and 17%, respectively. Nevertheless, the Young's modulus hardly changes with the vacancy size. When compared with the results of previous studies on carbon nanotubes using MD [9], molecular mechanics (MM) [10], and quantum mechanics (QM) [11] calculations, the reductions in the tensile strength of graphene with a single and double vacancy in this work are close to the results obtained with the MM and QM calculations.

Snapshots of the tensile loadings are shown in Fig. 9. For pristine graphene, the distribution of stress just before the fracture is uniform and the level of stress is high. In comparison, in the vacancy-containing graphene, the concentration of stress occurs around the vacancy just before the fracture, which emerges from the circumference of the vacancy.

TABLE II
TENSILE STRENGTHS OF VACANCY-CONTAINING GRAPHENE AND CNT

	Graphene	CNT(Carbon Nanotube)		
	σ_B (MD, GPa)	σ_B [9] (MD, GPa)	σ_B [10] (MM, GPa)	σ_B [11] (QM, GPa)
Pristine	91	104	105.5	135
Single vacancy	75 (-17%)	103 (-1%)	70.4 (-33%)	100 (-26%)
Double vacancy	64 (-29%)	101 (-3%)	71.3 (-32%)	105 (-22%)
Sextuple vacancy	65 (-28%)	—	—	—

σ_B is the tensile strength. Values in parentheses represent the differences between the pristine and vacancy-containing materials. MD, MM, and QM refer to Molecular Dynamics, Molecular Mechanics, and Quantum Mechanics, respectively. The [5,5] CNTs whose tensile direction agrees with the zigzag tension are used for all of the carbon nanotube results.

TABLE III
THE YOUNG'S MODULI OF VACANCY-CONTAINING GRAPHENE (UNIT: GPA)

Pristine	794
Single vacancy	782 (-1.5%)
Double vacancy	765 (-3.6%)
Sextuple vacancy	767(-3.4%)

Values in parentheses represent the differences between the pristine and vacancy-containing materials.

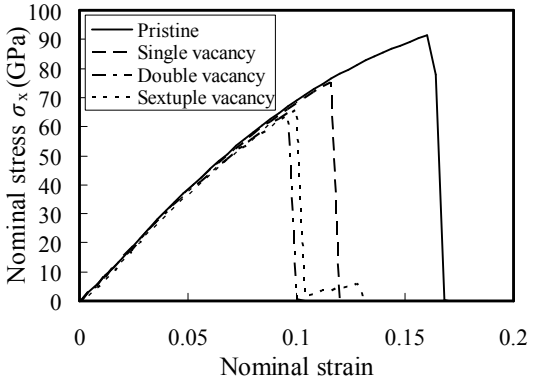

Fig. 8 Stress-strain curves of the graphene containing a cluster-type vacancy under zigzag tension.

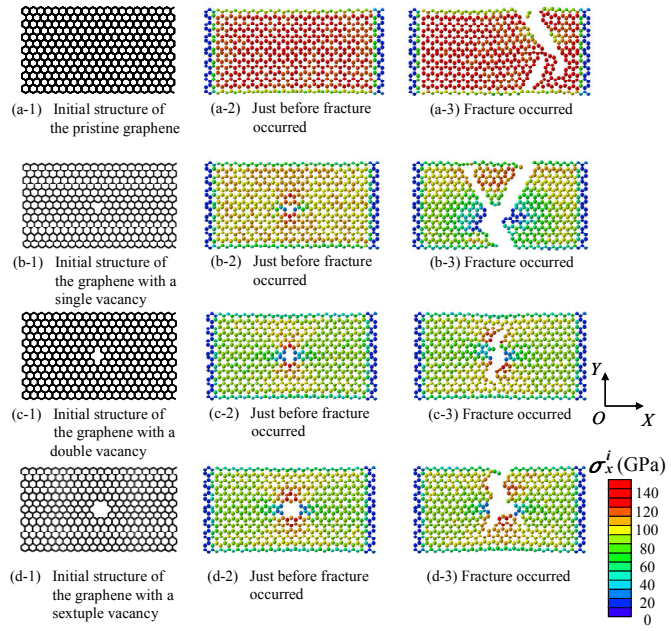

Fig. 9 Stages of fracture progression in graphene containing cluster-type. vacancy. (a-1)–(a-3): pristine, (b-1)–(b-3): single vacancy, (c-1)–(c-3): double vacancy, (d-1)–(d-3): sextuple vacancy.

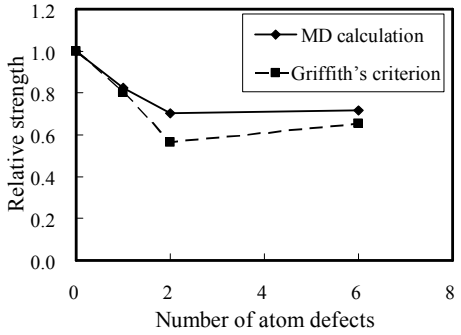

Fig. 10 Relative strengths and sizes of vacancy, namely, the number of atom defects obtained using MD calculation and Griffith's criterion.

We compared the calculated results with the Griffith's criterion in order to verify the propriety. The theoretically ideal strength σ_{max} for brittle fracture is expressed as

$$\sigma_{\max} = \sqrt{\frac{E\gamma_s}{d}}, \tag{6}$$

where E is Young's modulus, γ_s is the surface energy, and d is the interatomic distance. Then, the strength of materials containing a fracture of length 2C according to the Griffith's criterion is expressed as

$$\sigma_f = \sqrt{\frac{2E\gamma_s}{\pi C}}, \tag{7}$$

The relative strength σ_{rel}, that is, the strength of the materials with a fracture relative to the theoretically ideal strength is obtained by dividing σ_f by σ_{max} as

$$\sigma_{rel} = \sqrt{\frac{2d}{\pi C}}, \tag{8}$$

A plot of the relative strength against the number of atomic

ISBN: 978-988-19251-1-4
ISSN: 2078-0958 (Print); ISSN: 2078-0966 (Online)

defects is shown in Fig. 10. The results of MD calculations agree well with the predicted values using the Griffith's criterion.

C. *Influence of distributional form of defects*

For the graphene with uniformly or randomly distributed vacancies, the relationship between the tensile strength and the density of vacancies is shown in Fig. 11. For the random vacancy distribution, the average values of the two results calculated using the models with different vacancy arrangements are plotted. The error bar (I) represents the range between two values. The tensile strength decreases with the increase in vacancy density. The reduction in the tensile strength is 59% at a density of 4% for the random vacancy distribution. This is nearly twice that of the reduction in the tensile strength of hydrogen (H)-functionalized graphene [16]. In comparison, the Young's modulus slightly decreases with the increase in the vacancy density (see Fig. 12). The reduction in the Young's modulus is 20% at a density of 4%. This is nearly 4 times that of the reduction in the Young's modulus of H-functionalized graphene. It is reasonable to assume that graphene is more sensitive to vacancies than to H–coverage, because a vacancy implies the lack of an atom, whereas H-coverage refers to the conversion of local carbon bonding from sp^2 to sp^3 hybridization.

Snapshots of the graphene with uniformly distributed vacancies during tensile loading are shown in Fig. 13. In every case, the concentration of the stress occurs around each vacancy just before the fracture in the same manner as for the graphene with a single vacancy. Then, fractures occur starting from a vacancy and progress toward neighboring vacancies. The progression of the fracture direction is perpendicular to the tensile axis in all cases. Conversely, snapshots of the graphene with randomly distributed vacancies during the tensile loading are shown in Fig. 14. The fracture starts from the area where the vacancies gather. The progression direction of the fracture is then random.

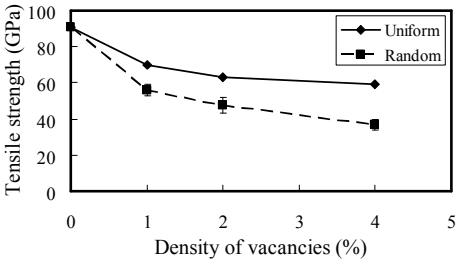

Fig.11 Tensile strength of graphene against vacancy density.

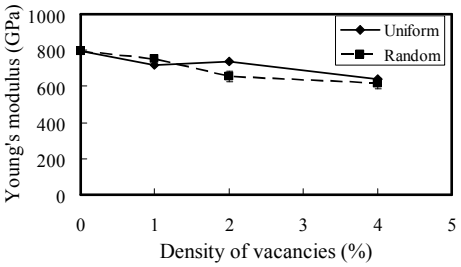

Fig.12 Young's modulus of graphene against vacancy density.

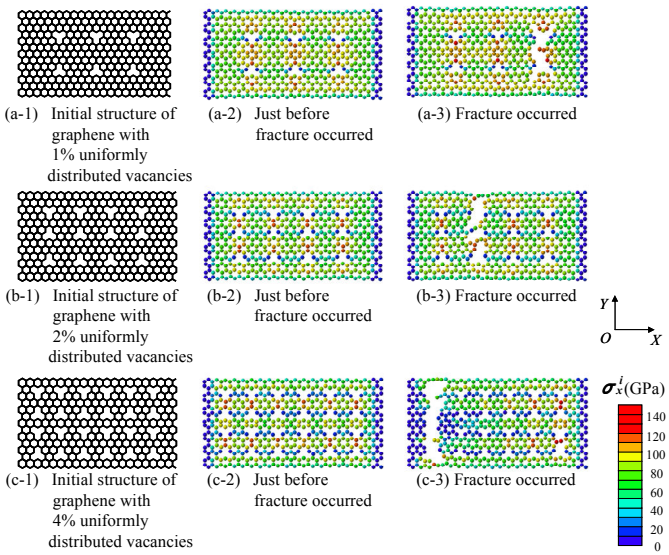

Fig. 13 Stages of fracture progression in graphene containing uniformly distributed vacancies. The density of vacancies is 1% ((a-1)–(a-3)), 2% ((b-1)–(b-3)), and 4% ((c-1)–(c-3)).

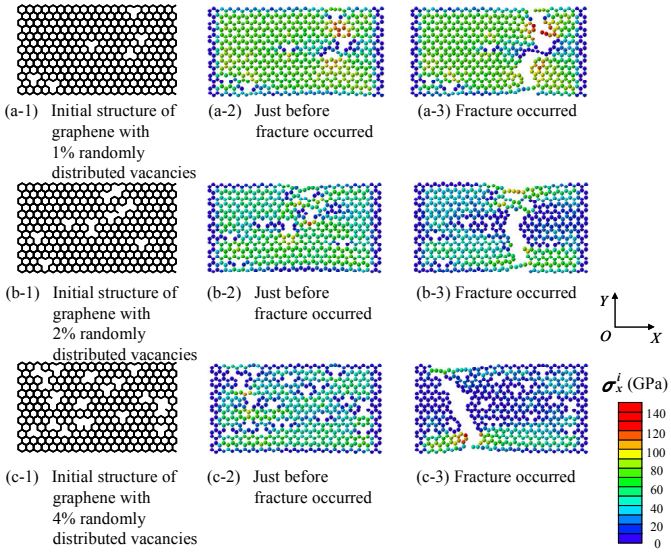

Fig. 14 Stages of fracture progression in graphene containing randomly distributed vacancies. The density of vacancies is 1% ((a-1)–(a-3)), 2% ((b-1)–(b-3)), and 4% ((c-1)–(c-3)).

D. *Mechanical properties of vacancy-containing graphite*

The stress and strain curves of graphite with a cluster-type vacancy at 300 K are shown in Fig. 15. The results for pristine graphite are also given for reference. In every case, reductions in stress occur before the fracture. For the single vacancy, the reduction occurs twice before the fracture, which occurs during the last stress peak; for the other vacancies, the reduction occurs only once.

Snapshots of the graphite with a cluster-type vacancy are shown in Fig. 16. It was found that the reduction in stress before the fracture was due to a tear in the graphene sheet. For the single vacancy, the first reduction in stress is due to the tearing of the vacancy-containing center layer ((a-1) and (b-1)). Then, the second reduction is due to the tearing of a neighboring layer ((a-2) and (b-2)). In this case, the atom in the broken piece of the center layer reacts with the atom at the edge of the neighboring layer and leads to the tearing of the neighboring layer by disturbing the zigzag edge surface (see

ISBN: 978-988-19251-1-4
ISSN: 2078-0958 (Print); ISSN: 2078-0966 (Online)

Fig. 17).

The relationship between the tensile strength of the center layer with a cluster-type vacancy in the graphite and the tensile strength of the graphene with a cluster-type vacancy is shown in Fig. 18. For all types of vacancy, the tensile strength of the center layer is almost equal to that of the graphene with a similarly sized vacancy. This means that the interlayer interaction hardly affects the tensile strength of the vacancy-containing center layer.

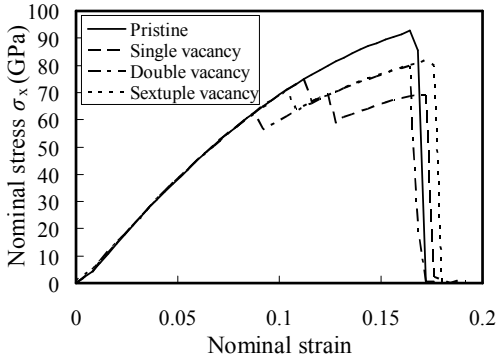

Fig. 15 Stress-strain curves of graphite containing cluster-type vacancy under zigzag tension.

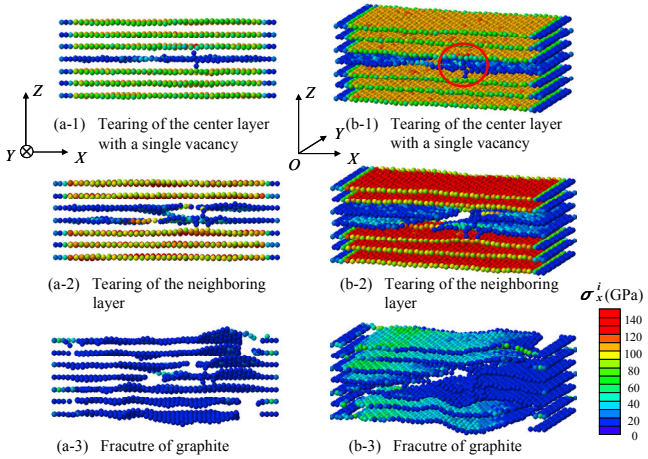

Fig. 16 Stages of fracture progression of graphite with single vacancy ((a-1)–(a-3): viewed in the Y direction, (b-1)–(b-3): viewed in the direction of slant.)

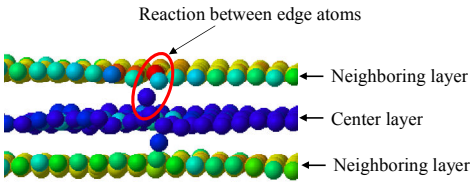

Fig. 17 Enlargement of circled section shown in Fig. 16(b-1).

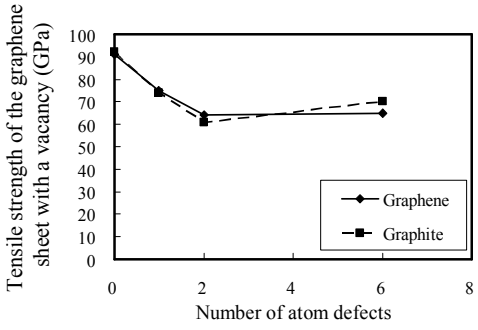

Fig. 18 Tensile strength of graphene with vacancy and of the vacancy-containing center in graphite, depending on the size of the vacancy, namely, the number of atomic defects.

IV. Conclusion

We performed MD simulations of tensile loadings on vacancy-containing graphene and graphite to investigate the influence of vacancies on the mechanical properties. It was found that for the cluster-type vacancy, the relationship between the size of the vacancy and the tensile strength agree with the relationship predicted using Griffith's criterion. We demonstrated that the difference in the distributional form of vacancies affects the tensile strength. In addition, it was found that there is not a large difference between the tensile strengths of vacancy-containing graphene and that of a graphene sheet in graphite containing a vacancy of a similar size.

References

[1] C. Lee, X. Wei, J. W. Kysar, J. Hone, "Measurement of the Elastic Properties and Intrinsic Strength of Monolayer Graphene," *Science*, vol. 321, pp. 385-388, Jul., 2008.

[2] H. –L. Zhang, S. –F. Wang, R. Wang, J. Jiao, "The Dislocations in Graphene with the Correction form Lattice Effect," *European Physical Journal B*,vol.73, pp. 489-493, Feb., 2010.

[3] S. K. Georgantzinos, G. I. Giannopoulos, N. K. Anifantis, "Numerical Investigation of Elastic Mechanical Properties of Graphene Structures," *Materials and Design*, vol. 31, pp. 4646-4654, Dec., 2010.

[4] P. A. Thrower, "The Study of Defects in Graphite by Transmission Electron Microscopy," *Chemistry and Physics of Carbon*, vol.5, pp. 217, 1969.

[5] A. Hashimoto, K. Suenaga, A. Gloter, K. Urita, and S. Iijima, "Direct Evidence for Atomic Defects in Graphene Layers," *Nature*,vol.430, pp.870-873, Aug., 2004.

[6] J. Osing and I. V. Shvets, "Bulk Defects in Graphite Observed with a Scanning Tunnelling Microscope," *Surface Science*, vol.417, pp.145–150, Nov., 1998.

[7] J. R. Xiao, J. Staniszewski, J. W. Gillespie Jr., "Tensile Behaviors of Graphene Sheets and Carbon Nanotubes with Multiple Stone-Wales Defects," *Materials Science and Engineering A*, vol. 527, pp. 715-723, Jan., 2010.

[8] R. Grantab, V. B. Shenoy, R. S. Ruoff, "Anomalous Strength Characteristics of Tilt Grain Boundaries in Graphene," *Science*, vol. 330, pp. 946-948, Nov., 2010.

[9] C. H. Wong, "Elastic Properties of Imperfect Single-walled Carbon Nanotubes under Axial Tension," *Computational Materials Science*, vol. 49, pp. 143-147, Jun., 2010.

[10] S. Zhang, S. L. Mielke, R. Khare, D. Troya, R. S. Ruoff, G. C. Schatz, and T. Belytschko, "Mechanics of Defects in Carbon Nanotubes: Atomistic and Multiscale Simulations," *Physical Review B*, vol. 71, pp. 115403, Mar., 2005.

[11] S. L. Mielke, D. Troya, S. Zhang, J-L Li, S. Xiao, R. Car, R. Ruoff, G. C. Shatz, and T. Belytschko, "The Role of Vacancy Defects and Holes in the Fracure of Carbon Nanotubes," *Chemical Physics Letters*, vol. 390, pp. 413, Apr., 2004.

[12] D. W. Brenner, O. A. Shenderova, J. A. Harrison, S. J. Stuart, B. Ni, S. H. Sinnott, "A Second-generation Reactive Empirical Bond Order (REBO) Potential Energy Expression for Hydrocarbons," Journal of Physics Condensed Matter, vol. 14, pp.783-802, Jan., 2002.

[13] O. A. Shenderova, D. W. Brenner, A. Omeltchenko, X. Su, L. H. Yang and M. Young, "Atomistic modeling of the fracture of polycrystalline diamond," Physical Review B, vol. 61, no. 6, pp.3877-3888, Feb., 2000.

[14] S. J. Stuart, A. B. Tutein and J. A. Harrison, "A reactive potential for hydrocarbons with intermolecular interactions," Journal of Chemical Physics, vol. 112, no. 14, pp. 6472-6486, Jan., 2000.

[15] L.V. Woodcock, "Isothermal molecular dynamics calculations for liquid salts," Chemical Physics Letters, vol.10, pp. 257-261, Aug., 1971.

[16] Q.X. Pei, Y.W. Zhang, V.B. Shenoy, "A molecular dynamics study of the mechanical properties of hydrogen functionalized graphene," Carbon, vol. 48, pp. 898-904, Mar., 2010.

[17] F. Liu, P. Ming, and J. Li, "Ab initio calculation of ideal strength and phonon instability of graphene under tension," *Phys. Rev. B*, vol. 76, pp. 064120, Aug., 2007.

[18] J.-W. Jiang, J.-S. Wang and B. Li, "Young's modulus of graphene: A molecular dynamics study," *Phys. Rev. B*, vol. 80, pp. 113405, Sep., 2009.

ISBN: 978-988-19251-1-4
ISSN: 2078-0958 (Print); ISSN: 2078-0966 (Online)